On the relationships between topography and gloss

Harold Lipshitz, Mark Bridger,[1] and Gary Derman
Derma-Metrics, 18 North Rd., Bedford, Mass. 01730

ABSTRACT *A newly developed system for characterizing the topographies of surfaces was used on three coated sheets that differed in gloss. In this system, the heights, z, of closely spaced points on a surface are determined as a function of their x,y coordinates in a reference plane [i.e., z (x,y)]. From these data, statistical distributions of a number of topographic parameters were determined. These include distributions of height density, relative area, and the regional inclinations across each surface (with respect to a reference plane). The distribution of these regional inclinations were called the "facet angle distribution" of the surface. Changes in the average facet angle and the breadths of the facet angle distributions correlated with changes in gloss. Measures of average roughness did not correlate with the loss of gloss when the surfaces were close in roughness. An improved way to use the facet angle parameter is suggested.*

KEYWORDS
Coated papers
Coatings
Gloss
Optical properties
Reflectance
Statistical distribution
Topography
Topography characterization

Gloss, though not precisely defined in the relevant literature (*1*), is a function of a surface's inherent reflectivity (*2*) and its specular and diffuse reflectances (*3-6*). Both the specular and diffuse reflectances of a surface are functions of its topography (*3, 4*). Though gloss and roughness are frequently reported to be inversely related (*7, 8*), it has proven difficult to correlate relative gloss with quantitative determinations of specific geometric characteristics of the surface. Therefore, this study was undertaken to identify measurable surface geometric parameters that relate to gloss.

Using a newly developed apparatus, we determined statistical distributions of a number of topographic parameters for three identically coated sheets that differed only in topography and gloss. The factors that affect the topography and gloss of coated sheets also relate to other practical problems in paper manufacturing (*9-11*). These include print mottling, "orange peel" gloss striations, coating graininess, ink density variations, coating mass variations, and gloss profile (*9-11*).

The topographical features that give rise to some of these effects have been reported to be on the submillimeter scale; that is, they range in size from 1 μm to 1 mm (*9*). To characterize them, the instrumentation has to be able to quantitatively measure three-dimensional topographical features in this relief range, at that scale, over relatively large areas.

It is our hope to use the techniques of this study to identify and characterize topographic parameters as they are related to practical problems in papermaking.

Procedures and results

Samples studied

The samples of coated paper were supplied by the Fortifiber Corp. of Attleboro, Mass. The basestock was a fine, clay-coated, bleached kraft paper, to which a 38-μm-thick coating of polypropylene was applied. The coating was applied by extrusion from the melt.

The sheets were machine calendered with a roller that had three sections differing in surface finish. One section had a "mirror" finish, and the other two were each slightly rougher. Because the three surfaces were calendered simultaneously, the average pressure and temperature during calendering were identical. The topographies of the calender surfaces were not characterized, and no characterization data were available for the polypropylene.

The sheets calendered with the mirror finish surface were quite glossy. The other two were successively less glossy. We will refer to the most glossy sheet as No. 1, and the others will be identified as Nos. 2 and 3, in order of decreasing gloss.

Relative gloss was measured with a reflectance meter at an angle of 45°. Defining the gloss of Sample 1 as 1.0, Samples 2 and 3 had gloss values of 0.8 and 0.5, respectively.

Data acquisition

The topographic characteristics of the coated samples were measured using

[1] Bridger is also associated with Northeastern University, Dept. of Mathematics, Boston, Mass. 02115.

instrumentation developed in our laboratory (patent pending). The system is based on the general principle that the focusing of a narrow beam of light on a small region of surface, inclined at a specific angle, results in a reflected diffuse image of the surface profile. Positions along the reflected image, as observed on a video detector, depend on the heights from which they are reflected.

From these reflected images, image processing hardware and software are used to obtain actual heights of the surface above a rectangular grid of points (x,y) in the reference plane (**Fig. 1**). This requires that positions be precisely located and calibrated against real distances. Denoting heights by z, and rows and columns (in the reference plane) by y and x respectively, the heights obtained are denoted as $z = z\,(x,y)$.

In this procedure, the test surface is scanned in a series of equally spaced rows—conveniently 128 rows with 256 equally spaced data points in each row. Scanning is performed automatically by computer-controlled stepper motors. Distances between points are variable and generally depend on the size of the area being characterized. These distances can be less than a micron between points. Heights can be determined to within 0.3 μm. However, the magnitude of the relief changes that can be measured is not practically limited, so that both rough and smooth surfaces can be characterized. Proprietary software and hardware are used to suppress noise and maintain focus while measurements are made over uneven surface terrain.

The data obtained constitute a matrix of height measurements as a function of their x, y coordinates in the reference plane (Fig. 1). Since it is difficult to attain precise orientation of the regions of the test surface with respect to the reference plane, we level our data in the following way. From the grid of points, we find the equation for the mean plane bisecting all points by least squares regression:

$$z = R(x,y) \qquad (1)$$

We then replace the heights, $z = z\,(x,y)$ by the new heights defined by

$$z = z\,(x,y) - R\,(x,y) \qquad (2)$$

Thus, all new heights are measured above or below the mean regression plane with points on the plane having the height 0. This procedure renders the mean plane parallel to the instrument reference plane and permits us to compare data from different samples and from different regions of the same sample.

Coordinate data obtained in this way, when plotted three dimensionally, yield facsimile images that are in excellent agreement with optical and scanning electron micrographs (SEM) of the same surface. Shading in the facsimile images results from a combination of point densities within a region and the use of a hidden line removal algorithm. The software further permits the researcher to obtain coordinates of specific surface features interactively. Heights and depths read in this manner agree closely with those computed from stereoscopic SEM data.

1. Diagram of the reference plane and measured distances

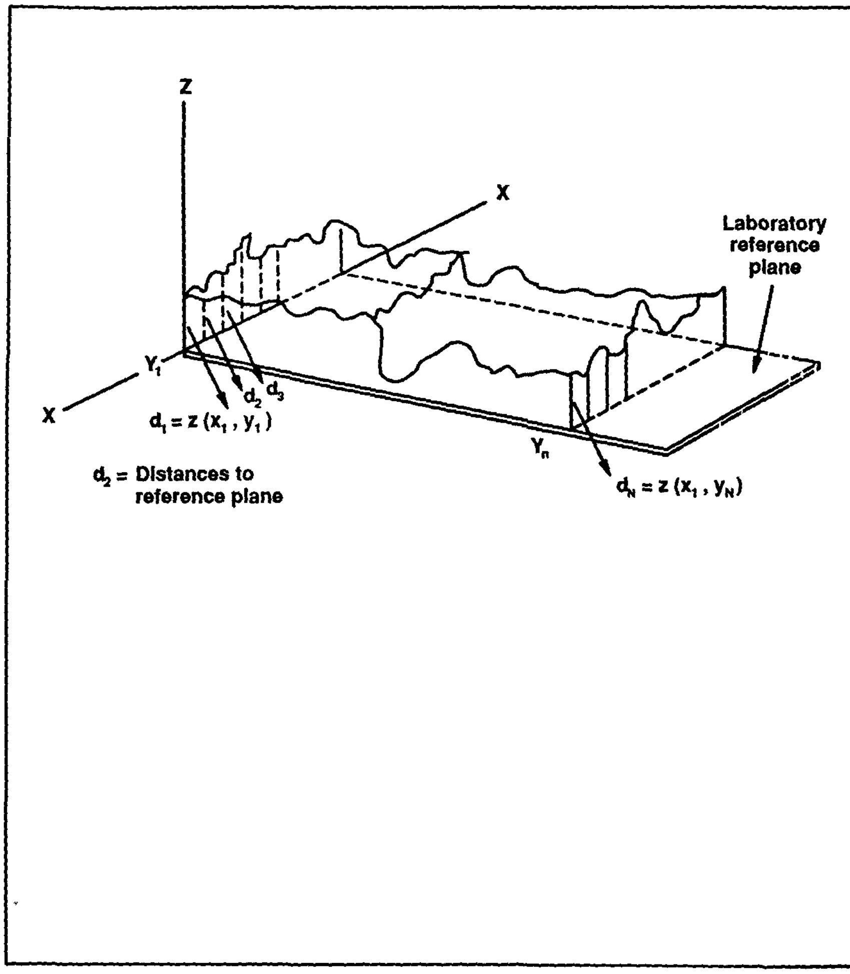

Facsimile images generated from data with different spacings between points

Facsimile images of Surfaces 1, 2, and 3, obtained from three-dimensional plots of coordinate data, are shown in **Figs. 2-4**. The z axes are expanded for better visualization of surface features. Expansions are the same for each comparable figure. (All of the frames labeled "A" for Figs. 2-4 are at the same expansion, as are all Frames B, C, and D.)

The figures of each group were obtained from data points having different spacings between them. The distances between points for Frames A, B, C, and D of each group are respectively 2.4, 5.3., 10.1, and 20.5 μm between rows (in the y direction) and 1.3, 2.6, 5.3, and 10.1 μm between points of each row (in the x direction). The characterized areas of each figure of each group are respectively 0.09.

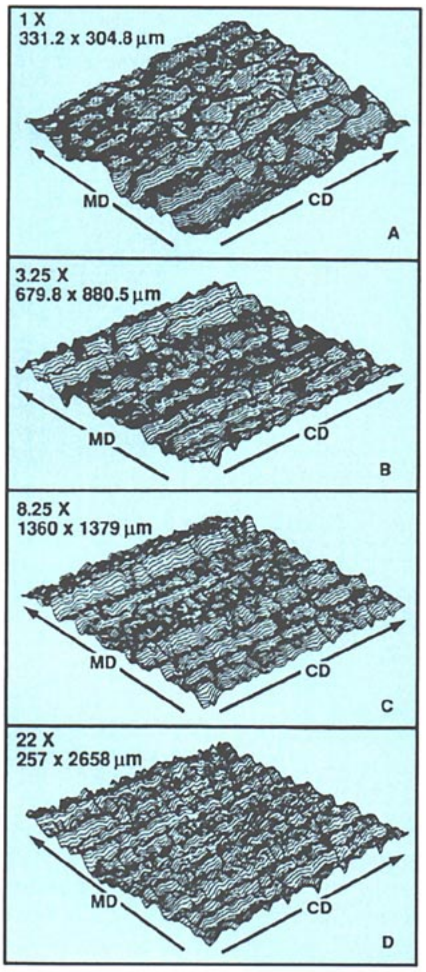

2. Facsimile images of surfaces of Sample 1. Distances between rows and columns: (A) 2.4 and 1.3 μm. (B) 5.4 and 2.3 μm. (C) 10.9 and 5.3 μm. (D) 20.8 and 10.1 μm.

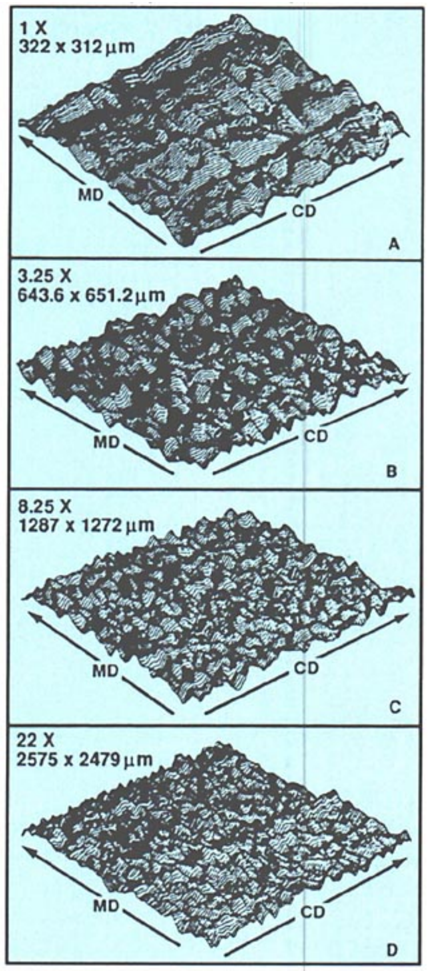

3. Facsimile images of surfaces of Sample 2. Distances between rows and columns: (A) 2.6 and 1.3 μm. (B) 5.1 and 2.6 μm. (C) 10.9 and 5.2 μm. (D) 20.6 and 10.1 μm.

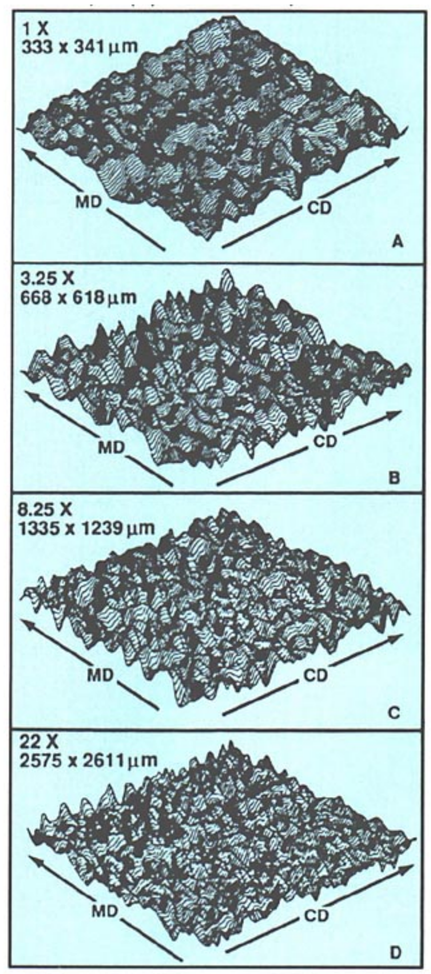

4. Facsimile images of surfaces of Sample 3. Distances between rows and columns: (A) 2.6 and 1.3 μm. (B) 5.3 and 2.6 μm. (C) 10.0 and 5.9 μm. (D) 19.5 and 10.1 μm.

0.45, 1.65, and 6.52 mm^2. The data for each region were obtained from different parts of the sheet.

Quantitative measures of surfaces featured were obtained directly from the facsimili images. The topography of Surface 1 is heterogeneous, with different regions having different topographical characteristics (Fig. 2). Periodic compressions and ridges cross each of the characterized regions. These regions are spaced between 230 μm and 350 μm apart. The ridges, which average 4-6 μm above the mean plane, are approximately 75-150 μm wide. From 1 to 3 ridges occur in series. Note that the surfaces in the ridge regions are relatively smooth.

Between the ridges are rougher regions approximately 300 μm wide. These are characterized by surface waves, many of which are oriented perpendicular to the machine direction. (In other words, the lines perpendicular to the crests are oriented perpendicular to the machine direction, or the calendering direction.) A smaller fraction of the waves are oriented between 30° and 45° with respect to the cross direction. The crests range in length from 75 μm to 150 μm and terminate where the ridges begin.

Surface 2 is less heterogeneous than Surface 1, having fewer regions with distinctly different topographic characteristics. Relatively flat plateau regions, at a size of around 50 × 75 μm, are interspersed among the wave-like structures. Again, the waves are predominantly oriented perpendicular to the machine direction. The crests are somewhat longer than those seen on Surface 1, ranging in length from 90 μm to 500 μm. While some ridges remain evident (Fig. 3A), they are considerably less pronounced than those of Surface 1.

Surface 3, the least glossy of the three, consists of wave patterns that, again, are predominantly oriented perpendicular to the machine direction. The amplitudes, frequencies, and average angles of descent of these surface oscillations are greater than those seen on the other two surfaces (Figs. 4B-D). The average angles of descent in the machine direction are less than those in the cross direction.

The topography of Surface 3 is generally more homogenous, meaning that similar features are present in all regions. The periodic ridges seen on Surface 1 and to a much lesser extent on Surface 2 are not evident in the image of Surface 3.

The images of the surfaces have similar features, regardless of the distances between points, or regardless of scale. That this is so is not obvious, since more information is

5. Height distributions of Surfaces 1, 2, and 3. Coordinate data were spaced 10.1 μm apart by columns and around 20 μm apart by rows.

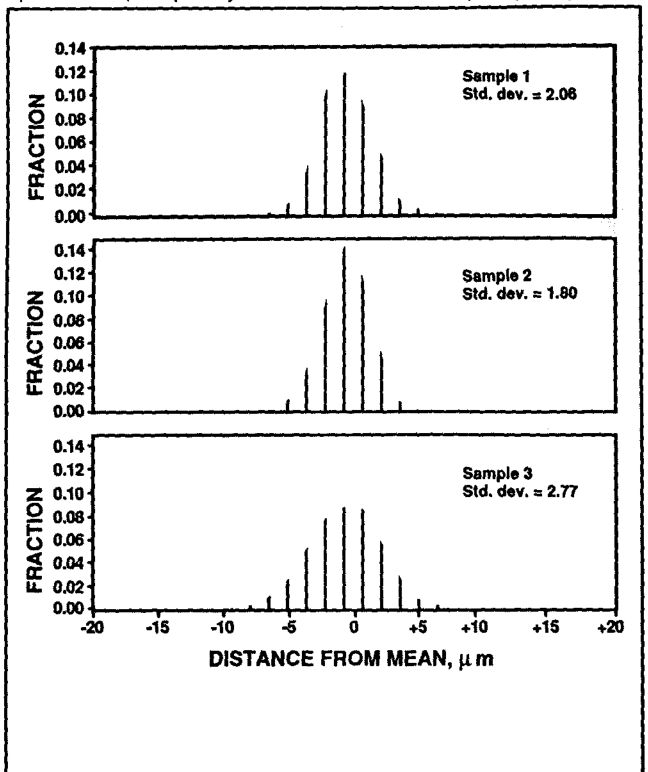

6. Height distributions of Surfaces 1, 2, and 3. Coordinate data were spaced 1.3 μm apart by columns and around 2.5 μm apart by rows.

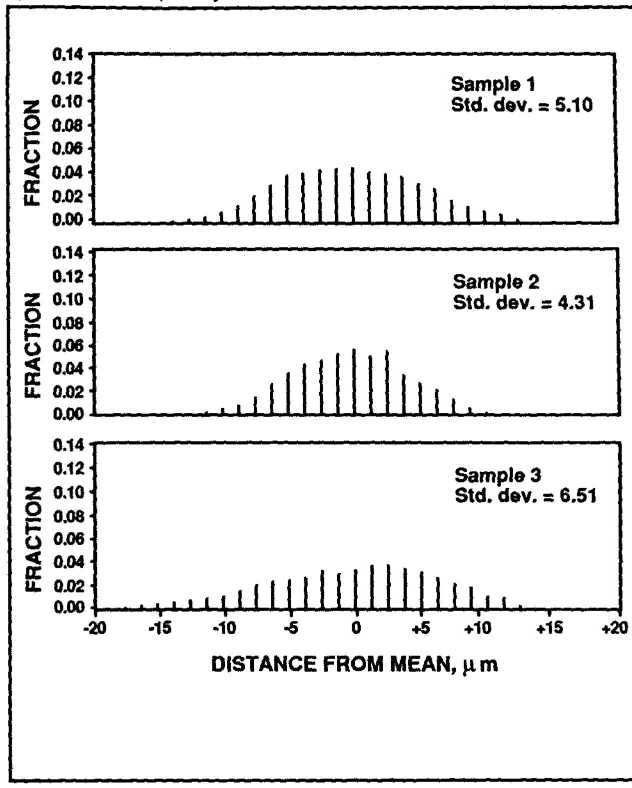

encompassed in curves obtained with more closely spaced coordinate data (see sections on height distributions and relative areas).

Height distributions

Figures 5 and 6 show the distributions of heights from the mean planes. The ordinates are the fractions of all points within a specific height range. The heights for each bar span 0.6 μm for both Fig. 5 and 6. By integrating these probability density distributions, we obtain the first-order distribution functions of the heights.

In Fig. 5, the height density distributions are plotted for coordinate data, spaced 10 and 20 μm apart in the x and y directions. In Fig. 6, the coordinate data were around 1.3 and 2.5 μm apart in the x and y directions.

As shown, the height density distributions for data sampled 10 and 20 μm apart appear Gaussian and narrowly distributed. These heights range from $\pm$ 6 to $\pm$ 9 μm from the mean plane. The distributions of Surface 2 are narrower, however, than those of Surface 1. The standard deviations for both data sets are less than those for Surface 1, despite the lower gloss of Surface 2. (Here, standard deviations are equal to the root mean square heights (RMS) of the surfaces, since the means are by definition equal to 0.)

The height distributions obtained from the more closely spaced data (Fig. 6) are by contrast at least trimodal (note that there are at least three peaks in each distribution), considerably broader, and asymmetric. Their range is from -20 μm to + 14 μm. Thus, the amplitudes of the higher frequency oscillations of these surfaces are considerably greater than those at lower frequency.

Relative areas and relative area distributions

The relative area is defined here as the computed surface area divided by its projected area in the x,y plane. It is a measure of a surface's average roughness. The "true" relative area of a surface is a parameter often found in theoretical treatments of the topographical effects on limiting contact angle measurements (*12*, *13*) and contact angle hysteresis (*14*). The smaller the distance between data points, the closer do the computed relative areas approximate the "true" relative areas. If these approach limiting values, as the distance between points decreases, then such determinations can yield close approximations to the "true" relative areas. (See the discussion section for more.)

The surface areas for each data set are calculated by joining groups of three adjacent data points, forming triangles. This divides the surface into triangular facets. Simple cross-product formulas are used to find the areas of these facets. These areas are summed to approximate the sample's total surface area. Since the surface generally lies over a simple rectangle in the x,y plane, the projected area is simply the length times width (in microns) of the characterized region. The relative areas can thus be simply expressed as shown in Eq. 3:

$$RA = (1/N_A) \sum_i A_i \quad (3)$$

where

RA = relative area

A_i = area of each facet

N_A = the nominal or projected area of each region.

7. Distribution of local relative area densities for the surfaces of Samples 1, 2, and 3.

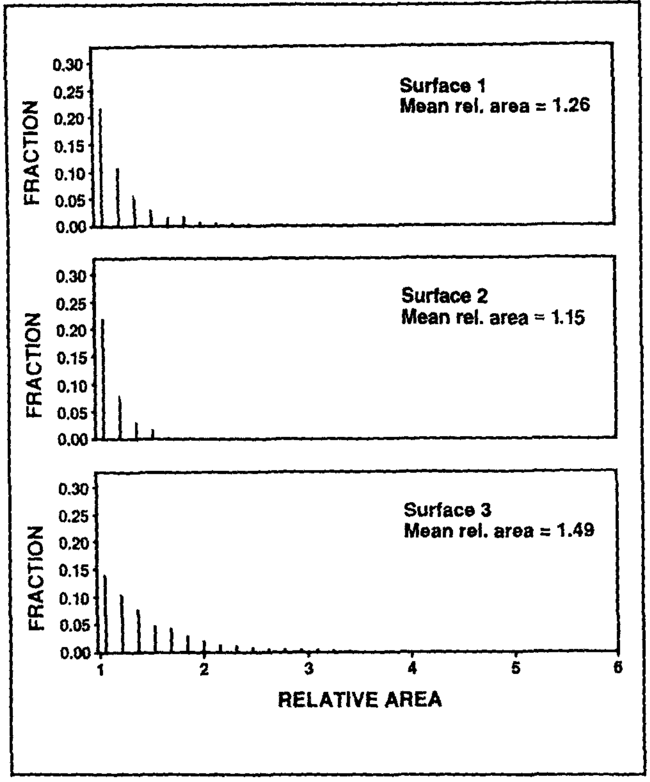

8. Diagram of the facet angle made between the cross-product vector and the mean reference plane, showing angles θ and ω.

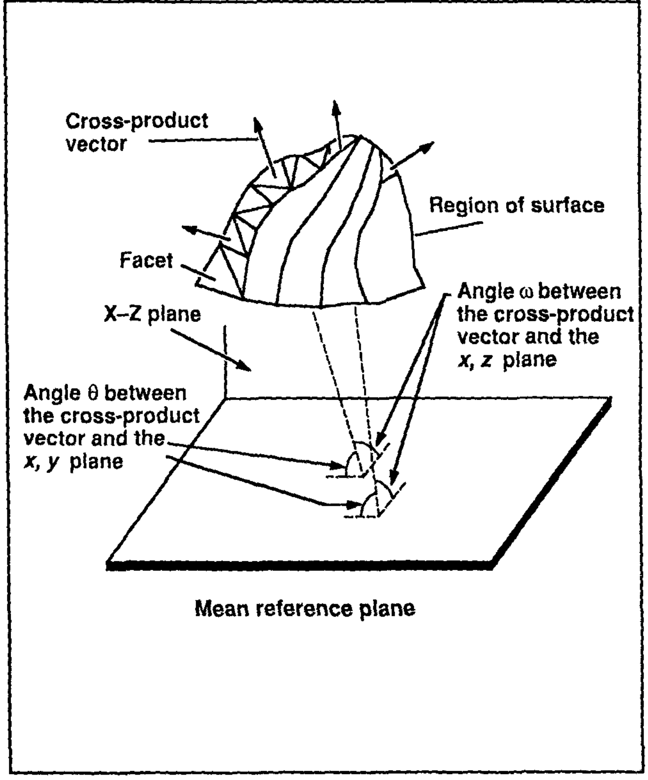

I. Relative areas and fractal dimensions of coated samples as determined with different spacings between points

Sample	Space between rows (y axis), μm	Space between points in rows (x axis), μm	Relative areas[a]	Fractal dimension[b]	Correlation coefficient
1	2.4	1.3	1.26	2.107	0.935
2	2.6	1.3	1.15	2.045	0.917
3	2.6	1.3	1.49	2.121	0.945
1	5.4	2.6	1.07	2.049	0.845
2	5.1	2.6	1.06	2.045	0.808
3	5.3	2.6	1.16	2.074	0.906
1	10.9	5.3	1.01	2.029	0.701
2	10.1	5.2	1.02	2.022	0.729
3	10.1	5.9	1.05	2.043	0.796
1	20.8	10.1	1.003	2.026	0.602
2	20.6	10.1	1.003	2.026	0.642
3	19.5	10.1	1.006	2.027	0.689

Values given are the means of three determinations
[a]Average deviation = 3.5%.
[b]Average deviation = 3%.

The relative areas of each sample for each data set are given in **Table I**.

More closely spaced points, detecting more oscillation, result in computed relative areas that increase as the distance between points decreases, as Table I shows. For each data set, however, the relative areas of Sample 3 are greater than the others, which is consistent with its having a rougher surface. However, the differences between Surfaces 1 and 2 are slight to none. In fact, by this criterion, Surface 2 appears less rough despite its lower gloss, which is consistent with the trend seen with the height density distributions.

More precise information is obtained by examining the distribution of relative areas. The breadths of these determinations serve as measures of roughness uniformity.

To make these determinations, the sample rectangular area is divided into a grid of smaller areas. (In this case, the analyzed area was divided into 3213 rectangular regions.) The relative areas of each small region are computed. The distributions for each surface are shown in **Fig. 7**, for the data most closely spaced. In these plots, the fractions of the areas in each span of relative area are plotted against the relative area.

While the differences between Surfaces 1 and 2 are small, the distribution of relative areas for Surface 1 is broader. Recall the greater heterogeneity of the topography of Surface 1 (Fig. 2). It appears that the broader distribution of Surface 1 causes Surface 2 to have an overall smaller relative area. Surface 3, the roughest and least glossy, has, as expected, lower fractions of smooth areas (that is, relative areas that approach 1) and the broadest distribution. Note that the relative area distribution curves decay exponentially.

Fractal dimension

Absolute true relative areas can only be determined at infinitely close points. Mandelbrot (*15*) has stated that such determinations cannot readily be made since areas measured using smaller and smaller scales increase exponentially (as we found for these surfaces). While this trend is found for a great number of surfaces, asymptotic limiting values of surface areas have been obtained with decreasing scales of measurement (*16, 17*) (as covered in the the discussion section). Generally, however, simple extrapolation to "zero" distance between points is not feasible.

Mandelbrot has proposed the use of a scaling parameter, termed the "fractal dimension," that relates measured real areas to measuring scale. He proposed that the scaling parameter obeys a simple exponential relationship having the form (*14, 18*):

$$A(\epsilon) = K\epsilon^{(2-D)} \quad (4)$$

where

$A(\epsilon)$ = surface area for measurement scale ϵ

K = a constant

D = the surface's fractal dimension.

The value of D can vary, in this case, between 2 and 3. A mathematically smooth surface has a value of D equal to 2, and the fractal dimension of a very rough surface approaches 3. Thus, the fractal dimension is by itself, when valid, a scale-independent measure of surface roughness. If the relationship of Eq. 4 holds, then plots of log $A(\epsilon)$ vs. log ϵ yield straight lines whose slopes are $(2 - D)$.

The calculation procedure is to compute the surface areas for each data set, with successively more alternate data points in the rows and columns left out. This procedure effectively changes the scale of the unit area for calculating $A(\epsilon)$. Determinations are done for 10 values, and the slopes of the least squares regression lines are calculated. The D values are obtained from the slopes.

Table I gives the fractal dimensions computed for each data set, with the correlation coefficients for each of the regression lines. As shown, the values of D, together with the correlation coefficients, increase with decreasing distance between the points. However, the goodness of fit is poor with distances between points greater than 1-2 μm.

It would appear that Eq. 4 does not describe these surfaces, although it holds for a wide variety of natural surfaces (*19*). The assumption inherent in Eq. 4 is that regardless of complexity, surface features are self similar and arise from some general rule. The lack of consistency between values obtained at different scales would give rise to the argument that these surfaces cannot be characterized by such a simple relationship.

It is noteworthy, however, that the images in Figs. 2-4 have similar features regardless of the scale or distance between data points. Furthermore, the topography of Surface 1 is heterogeneous, as are the topographies of the others, to lesser extents. It is therefore possible that if these surfaces are indeed fractal, an adequate description of their fractal nature requires more than one constant.

While the computed fractal dimensions of Surface 3 are greater than those of Surfaces 1 and 2, regardless of scale, the differences between Surfaces 1 and 2 are not discernible at any scale (i.e., perhaps more than one rule is operative). Indeed, for the closest spaced data, Surface 2 has a lower value of D, which would imply that it is less rough.

Facet angle distributions

The relationships between reflective scattering intensity and topography are complex (*3, 4, 20*). However, under the limiting conditions of rough surface approximations, which apply to even these relatively smooth surfaces, reflective scattering theory predicts that the magnitudes of reflectance, at given angles of measurement, relate to the orientations of "elemental" regions, with respect to the mean plane (*3, 4, 20*). Consequently, the localized scattering intensities of each region in effect map its slope distribution (*3,4*).

As stated, every three adjacent data points in the matrix are coordinates in our system of triangular facets which, taken together, approximate the topography of the surface. The orientation of each facet equals the average orientation of that area. Since gloss is a function of a surface's specular and diffuse reflectance (*3, 4*) and hence its slope distributions (*3*), we determined the orientation distribution of these facets for each surface.

The procedure was as follows. The intersection of two legs of each triangular facet constitutes the intersection of two vectors whose cross product is a vector perpendicular to the plane of the facet (**Fig. 8**). The orientation of the cross product vector with respect to the mean reference plane is described by two angles: θ_N, made with the x,y plane, and ω, made with the x,z plane.

Neglecting for these purposes orientations with respect to the x,z plane and angles greater than 90 degrees, all intersections with the x,y plane are described by the acute angles made with that plane. In this scheme, a facet oriented parallel to the mean reference plane has a facet angle of 90°, while facets, at the other extreme, oriented perpendicular to the x,y plane have a facet angle of 0°.

To obtain distributions, the number of facets having the same orientation are summed, then each angle is weighted by the total area of all facets at that angle. These are normalized by dividing by the sum of the areas of all facets, or by the total computed surface area. The operation is symbolically described by Eq. 5.

$$F_\theta = (1/\sum_i A_{Ni})\theta_N A_N = (1/A_S)\theta_N A_N \quad (5)$$

where

F_θ = normalized fraction of facet angles

9. Facet angle distributions for Surfaces 1, 2, and 3 for coordinate data spaced about 5.3 and 10.1 μm apart in the x and y directions

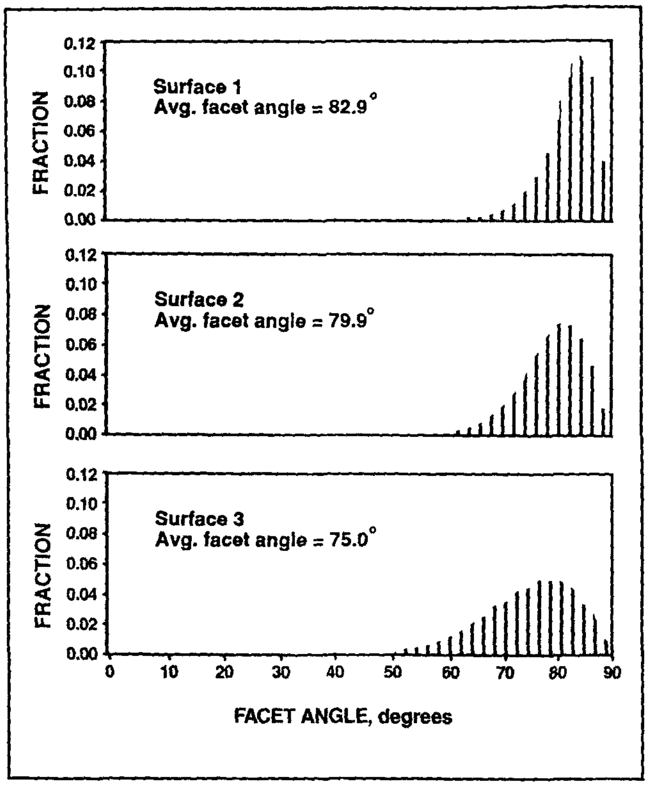

10. Facet angle distributions for Surfaces 1, 2, and 3 for coordinate data spaced about 2.5 and 5.3 μm apart in the x and y directions. (The scale of the ordinate is different from that of Fig. 9.)

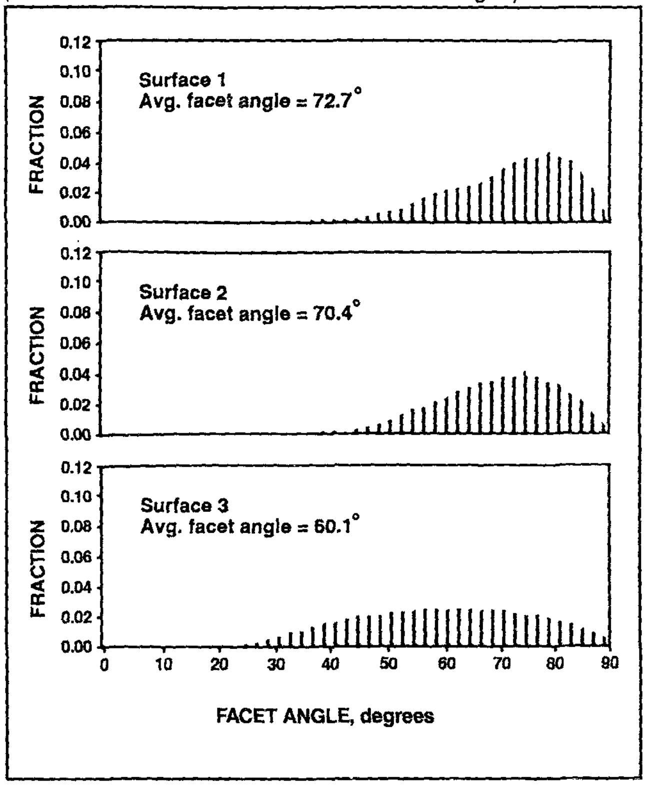

θ_N = angle formed by the normal to each facet with the reference plane

A_N = total area of all facets making the angle θ_N with the reference plane

A_S = total surface area of that region.

Facet angle distributions for Surfaces 1, 2, and 3 are shown in **Fig. 9** for data spaced approximately 5.3 and 10.9 μm apart. As shown, the average facet angles decrease from 82.9° for Surface 1 to 79.9° for Surface 2 to 75.0° for Surface 3. This decreasing order is consistent with the decreasing relative glossiness of the three surfaces. Accordingly, there is a greater preponderance of flatter facets, or areas of this size, on Surface 1 than on Surface 2, and more on Surface 2 than on Surface 3.

To reiterate, the orientation of each facet approximates the average orientation of that region of the surface. Thus, facet angle distributions are dependent on the average facet size used for analysis. Larger facets, obtained with data spaced further apart, average greater numbers of orientations. Within each facet the net effect is that the surface is modeled as having flatter regions or greater facet angles. Smaller facets, on the other hand, give greater weight to more orientations. This results in lower average facet angles and different distributions.

This is illustrated in **Fig. 10**, where the facet angle distributions for the three surfaces are shown for data spaced approximately 2.5 and 5.0 μm apart in the x and y directions. The facet angle distribution of Surface 1 is broader than that of Surface 2 and has a "plateau" region. This distribution is consistent with the greater heterogeneity of its topography as seen in the facsimile images and the height density and relative area distributions.

The facets of Fig. 9 had a minimum area of 25 μm^2, and analysis was done over 1.4 mm^2. Using these relatively large facets over this area, reproducible distributions were obtained for different regions of each surface. However, because of topographical heterogeneity, different distributions were obtained for different regions when smaller areas were analyzed. In addition, the average facet angles of Surface 2 were not always less than those of Surface 1. With data spaced at 5.3 and 10 μm over an analyzed area of 1.4 mm^2, the distributions were within 1% of each other from region to region. Apparently, with larger regions, topographical variations are averaged, and the surface is rendered more homogeneous.

Discussion of results

It seems evident that the often-stated inverse relationship between surface roughness and gloss (*7, 8*) does not always predict changes in gloss. All the topographic parameters of surface roughness in this study, except the facet angle determinations, indicated that Surface 2 was less rough than Surface 1 despite its lower gloss. It had narrower height density distributions, smaller standard deviations (or root mean square (RMS) values) at all scales, lower relative area ratios, and narrower relative area distributions.

It appears that the more fundamental topographic parameters related to gloss are those that measure the surface's average angular inclination with respect to the reference midplane and their distribution. The acquisition of closely spaced coordinate data, permitting calculations of average facet angles and facet angle distributions, provided the means of characterizing these important properties. It is probable that when surfaces differ significantly in roughness, that differences in their R_a (average deviation from the mean) or RMS (root mean square) values relate to changes in their average facet angle and facet angle distributions (as with Surface 3). However, the more fundamental parameters related to gloss seem to be those measuring angular inclination.

The correlation between changes in average facet angle and facet angle distribution with diminished gloss is not surprising in the light of known theories for the angular dispersion of reflected light from rough surfaces (*2-4, 20*). However, the topographic complexities of these coated and uncoated papers, their anisotropy, and regional variations add further complexity to the interpretation of these results.

Averaging of orientations

To obtain reproducible average facet angles and facet angle distributions from region to region, the analysis had to be done with facets having a minimum area of 25 μm^2, over approximately 1.4 mm^2. As stated, the use of these relatively large facets to model the surface resulted in the averaging of more orientations within each region than would have been the case with smaller facets, or those computed from more closely spaced data. The net result was that the surface was modeled as being more homogeneous than the true surface (that is, less subject to regional variations) and flatter than the true surface (the average facet angles being greater than those determined with smaller facets). Thus, the parameters derived from this model, while they correlated with the average changes in gloss, were based on a model somewhat removed from reality. In addition, the size of the facet needed to average small regional variations would probably not be the same for all surfaces.

Perhaps a more realistic model could be obtained if the reflective intensities of each region (or facet) at selected angles of measurement were correlated with that region's facet angle. This approach differs from what was done in this study, where correlations were drawn between "global" average values of inclination and "global" measures of reflective intensity. Direct, point-by-point correlation between each region's reflective intensity and its inclination would permit the use of smaller facets, having more homogeneous topographies within each facet. In addition, the size of the facets might be similar for most surfaces, provided the overall characterized areas were large enough to take into account large regional variations. This should result in derived parameters being obtained from a more realistic model of the surface's topography.

Such an approach would require measurements of the reflective intensities of each region and their superposition on mappings of angular inclination. Mappings of reflective intensity have recently been reported by Fujiwara *et al.* (*11*) but not at this resolution. We are presently pursuing this approach, and we hope to apply the results to problems of gloss profile and gloss variation.

Value of data from surface area characterizations

This study points to the importance of information derived from area characterizations as opposed to profilometry. As Nayak pointed out (*21*), peaks on profilometric traces probably do not correspond to the summits of actual surfaces. Of greater importance with regard to gloss is that measurements of distributions of angular inclination from traces are not the same as those for the surface. In his theoretical study of Gaussian surfaces (*21*), Nayak demonstrated that such assumptions lead to serious errors.

Along the same vein, the general presumption that statistical parameters derived from traces are equal to those derived from surface data seems particularly incorrect for these coated paper surfaces. The facsimile images of Surfaces 1 and 2 (Figs. 2 and 3) revealed regional variations in topography despite their relative smoothness. In addition, the three surfaces (Figs. 2-4) exhibited wave-like features with pronounced directionality. The forms of profilometric traces on these surfaces would therefore depend on the region analyzed and the direction of the trace (assuming there was sufficient lateral resolution).

Incidentally, the facsimile images produced during this study offered some distinct advantages over conventional micrographs in assessing topographical characteristics. In addition to being able to quantitatively measure the dimensional characteristics of specific features, we were able to observe, because of the absence of texture, geometric aspects of the surface that are not apparent in conventional micrographs. Of more importance, however, was the ability to expand one axis while keeping the others constant. This permitted visualization of surface features over relatively large fields. These features were not apparent without expanding the axis.

Further surface considerations

At spacings of 10 and 20 μm in the x and y directions, the height density distributions of the three surfaces were of Gaussian form (Fig. 5). The distances from the mean plane were within $\pm$ 9 μm. When the coordinate data were spaced at 1.3 and 2.5 μm in the x and y directions, the height density distributions were considerably broader, asymmetric, and at least tri-modal (Fig. 6). Therefore, for each of these surfaces, higher frequency oscillations of greater amplitude are superimposed on oscillations of smaller amplitude and lower frequency. These characteristics would not have been observed if the data were obtained only at a single sampling interval.

Since the oscillations of higher frequency are primarily responsible for the loss of gloss (these having the lowest facet angles), the data point to the importance of lateral resolution capabilities of around a micron or less in elucidating topographical characteristics of importance to gloss.

These surfaces were experimentally obtained by calendering with surfaces of different roughness. Calendering processes are very complex (*22*). However, these surfaces apparently resulted in part from localized flow during calendering, perpendicular to the calendering direction, and from annealing. As such, the surface topographies of the sheets would probably change with variations in the temperature, pressures, and speeds of calendering, the rheological properties of the polypropylene, and the deformational properties of the underlying clay-coated kraft paper. Hence, topographical analyses as functions of each of these process variables would be informative in trying to understand their effect on the sheets' overall topography.

Fractal dimensions

Because so many unrelated variables affect the topographies of the sheets, it would have been fortuitous if the topographies could have been characterized by a simple, one-constant scaling law. As stated, regional variations may have been partially responsible for the poor fit of the data to Eq. 2. The fact that the fit was better (having higher coefficients of correlation) when smaller regions were analyzed is supportive of this concept. It is therefore possible that different regions of the surface obey different scaling laws, and a more complicated scaling equation is required.

The right side of Eq. 2 has a negative exponent (except for the unrealistic case of a mathematically flat surface). Consequently, it predicts that the area of a surface is unbounded and that the area increases exponentially with decreasing scale. This abstraction is at variance with the concept that real surfaces have finite areas. Recent fractal data (*17*) have deviated from this Mandelbrot dictum. These data indicate that with decreasing scales of measurement, the areas or lengths converge to some "true" value. As a result, Underwood and Banerji (*16*) have proposed a new scaling law that uses the fractal dimension concept but provides that measured parameters approach limiting values with decreasing scale.

The importance of the fractal concept and its physical meaning for fibrous structures and coated surfaces has yet to be fully explored. A clearer understanding will require further analysis.

Summary

Closely spaced coordinate data were obtained using a new system for characterizing topography. These coordinate data consist of the heights of regularly spaced points on the surface as a function of their x,y coordinates in a reference plane.

The average facet angle and facet angle distributions calculated from these data provide a more fundamental topographic parameter related to gloss than generalized measures of roughness. The use of this parameter may be refined by directly correlating each small region's inclination with its reflective intensity measured at selected angles.

The microscopic topographies of seemingly smooth, glossy, coated sheets are actually complex. The topography of the glossiest sheet was heterogenous, with different regions having different topographical characteristics. Generalized measures of roughness did not predict the loss of gloss when the surfaces did not differ significantly in roughness.

The sheets were shown to have "gaussian"-like height distributions from the reference mid-plane when the coordinate data were spaced 10 μm and 20 μm apart in the x and y directions. On the other hand, the height distributions of more closely spaced data were considerably broader, and at least tri-modal. These findings illustrate the importance of the lateral resolution of height measurements of around a micron or less and the need to employ different sampling intervals when characterizing the topographies of glossy sheets.□

Literature cited

1. Westberg, J., Proc. Instn. of Mech. Engrs. 182(Part 3K): 260(1967/68).
2. Skilling, H. H., Fundamentals of Electric Waves, Wiley, New York, 1948, p. 138.
3. Church, E. L., Wear 57: 93(1979).
4. Clark, G. M. and Thomas, T. R., Wear 57: 107(1979).
5. Elmendorf, A. and Vaughan, T. W., J. Forest Prods. 8: 275(1958).
6. Hunter, R. S., J. Opt. Soc. Am. 36: 178(1946).
7. Van den Akker, J. A. and Sears, G. R., Tappi 47(11): 179A(1964).
8. Gate, L., Windle, W., and Hine, H., Tappi 56(3): 61(1973).
9. MacGregor, M. A. and Conners, T. E., Tappi J. 70(9): 95(1987).
10. Tomimasu, H., Suzuki, K., Toshimasa, O., and Luner, P., Tappi J. 73(5): 179(1990).
11. Fujiwara, H., Kaga, C., and Kano, I., 1990 Coating Conference Proceedings, TAPPI PRESS, Atlanta, p. 209.
12. Johnson, R. E. and Dettre, R. H., Adv. in Chem. Ser. 43: 112(1964).
13. Oliver, J. F., Huh, C., and Mason, S. G., Colloid Surface 1: 79(1980).
14. Andrade, J. D., Smith, L. M., and Gregoris, D. E., in Surface and Interfacial Aspects of Biomedical Polymers (J. O. Andrade, Ed.), Plenum Press, New York, 1985.
15. Mandelbrot, B. B., The Fractal Geometry of Nature, Freeman, N.Y., 1983.
16. Underwood, E. E. and Banerji, K., Mat. Sci. & Engr. 80: 1(1986). Coating Tech. 59: 35(1987).
17. Banerji, K., Met. Trans. 19A: 961(1988).
18. Martin, J. W. and Bentz, D. P., J. Coating Tech. 59: 35(1987).
19. Avnir, D., Farin, D., and Pfeifer, P., Nature 308: 261(1984).
20. Beckmann, P., The Scattering of Electromagnetic Waves From Rough Surfaces, Pergamon Press, London, 1963.
21. Nayak, P. R., Trans. ASME, J. Lub. Tech. 93F: 398(1971).
22. Tuomisto, M. V. and Sipi, K., Tappi J. 73(5): 131(1990).

We would like to thank Frank Banisch and Robert Jones of the Fortifiber Corp. of Attleboro, Mass., for providing the samples for study.

Received for review June 14, 1990.

Accepted June 26, 1990.

Presented at the TAPPI 1990 Polymers, Laminations and Coatings Conference.